

# Detailed Rapidity Dependence of $J/\psi$ Production at energies available at the Large Hadron Collider

Baoyi Chen

*Department of Physics, Tianjin University, Tianjin 300350, China*

(Dated: July 28, 2021)

$J/\psi$  suppression with rapidity is studied with both (3+1) dimensional transport equation and hydrodynamics in details at  $\sqrt{s_{NN}} = 2.76$  TeV Pb+Pb collisions. In central rapidity region of the hot medium,  $J/\psi$  nuclear modification factor shows weak rapidity dependence due to the boost invariance of the medium. But in forward rapidity region for entire transverse momentum bin,  $J/\psi$  regeneration is strongly suppressed due to the decreasing charm pair cross section. This makes  $J/\psi$   $R_{AA}(y)$  decrease with rapidity. The ratio  $r_{AA}$  of mean transverse momentum square in AA collisions to that in pp collisions increases strongly in forward rapidity region and is more sensitive to the  $J/\psi$  production mechanisms.

PACS numbers: 25.75.-q, 12.38.Mh, 24.85.+p

## I. INTRODUCTION

$J/\psi$  is a tightly bound state consisting of charm and anti-charm quarks. Its dissociation temperature is much higher than the critical temperature  $T_c$  of the deconfined phase transition. Therefore,  $J/\psi$  suppression has long been considered as a signature of the new state matter, the so-called Quark-Gluon-Plasma (QGP) [1]. Since then the production and suppression mechanisms of charmonium in QGP are widely studied [2–5]. The suppression from color screening of parton is supposed to be stronger with the temperature increasing. However, from the Au+Au data at the top colliding energy  $\sqrt{s_{NN}} = 200$  GeV of Relativistic Heavy Ion Collider (RHIC) [6], it seems that  $J/\psi$  suffer less suppression in central rapidity region than in the forward rapidity region of the hot medium, where the former one corresponds to a much higher temperature than the latter one [7–9]. This feature is much stronger at Large Hadron Collider (LHC). Even shadowing effect shows a strong rapidity dependence in pA collisions [10], it's almost rapidity independent in AA collisions [11]. And  $J/\psi$  regeneration [12] seems to be responsible for the rapidity dependence of  $J/\psi$  nuclear modification factor  $R_{AA}(y)$ . In this work, I combine both (3+1) dimensional Boltzmann type transport equation for charmonium evolution and (3+1) dimensional ideal hydrodynamics together, to describe detailed rapidity dependence of charmonium suppression, especially in the forward rapidity region at  $\sqrt{s_{NN}} = 2.76$  TeV Pb+Pb collisions.

In Section II, I introduce the transport model for charmonium suppression and regeneration in QGP. In Section III, I give detailed discussions about charmonium initial distribution and cold nuclear matter effects including shadowing effect and Cronin effect. I compare the theoretical calculations with the experimental data, and discuss the different rapidity dependence of parameters in the transport model in Section IV, and summarize the work in Section V.

## II. TRANSPORT MODEL

As charmonium is so heavy to be thermalized in the deconfined matter, I use a Boltzmann-type transport equation to describe the evolution of their phase space distribution  $f_\Psi(\mathbf{p}, \mathbf{x}, t|\mathbf{b})$  [13, 14],

$$\left[ \cosh(y - \eta) \frac{\partial}{\partial \tau} + \frac{\sinh(y - \eta)}{\tau} \frac{\partial}{\partial \eta} + \mathbf{v}_T \cdot \nabla_T \right] f_\Psi = -\alpha_\Psi f_\Psi + \beta_\Psi \quad (1)$$

where  $\Psi = (J/\psi, \chi_c, \psi')$ . The contributions from the feed-down of excited states  $\chi_c$  and  $\psi'$  to the final prompt  $J/\psi$  are 30% and 10% respectively.  $\tau = \sqrt{t^2 - z^2}$  is local proper time, and  $y = \frac{1}{2} \ln[(E + p_z)/(E - p_z)]$  and  $\eta = \frac{1}{2} \ln[(t + z)/(t - z)]$  are rapidities in momentum and coordinate spaces.  $\nabla_T$  indicates two dimensional derivative in transverse coordinate space.  $\mathbf{b}$  is the impact parameter of two colliding nuclei. Due to interactions with the hot medium, charmonium distribution  $f_\Psi(\mathbf{p}, \mathbf{x}, t|\mathbf{b})$  changes with time which is described in the first term at L.H.S of Eq.(1). The second term represents leakage effect, where charmonium with large transverse velocity  $\mathbf{v}_T = \mathbf{p}_T/E_T$  tend to suffer less suppression by free streaming from the hot medium,  $E_T = m_T = \sqrt{m_\Psi^2 + p_T^2}$  is charmonium transverse energy. When charmonium moving in the QGP, it may be dissociated by inelastic collisions with gluons, and the dissociation rate is described by the term  $\alpha_\Psi$  in Eq.(1),

$$\alpha_\Psi = \frac{1}{2E_T} \int \frac{d^3\mathbf{k}}{(2\pi)^3 2E_g} \sigma_{g\Psi}(\mathbf{p}, \mathbf{k}, T) 4F_{g\Psi}(\mathbf{p}, \mathbf{k}) f_g(\mathbf{k}, T) \quad (2)$$

where  $E_g$  is gluon energy,  $F_{g\Psi}$  is the flux factor.  $f_g = d_g/(e^{\frac{p_\mu u^\mu}{T}} - 1)$  is the gluon thermal distribution with the degeneracy  $d_g = 16$ .  $u_\mu$  is four velocity of the fluid. Due to strong color screening of QGP, the binding energy of  $J/\psi$  is reduced. The difference between quasifree dissociation ( $g, q + c \rightarrow g, q + c$ ) and photo-dissociation ( $g + J/\psi \rightarrow c + \bar{c}$ ) is large at high temperature [15–17]. However, their values are close to each other in the temperature region:  $0.2 \sim 0.3$  GeV [15]. Therefore, in this temperature region, one can employ the inelastic scattering cross section between  $J/\psi$  and gluon  $\sigma_{g\Psi}(0)$  in vacuum [18, 19], and obtain its value at finite temperature with geometry scale  $\sigma_{g\Psi}(T) = \langle r_\Psi^2 \rangle(T) / \langle r_\Psi^2 \rangle(0) \times \sigma_{g\Psi}(0)$ . The mean radius square  $\langle r_\Psi^2 \rangle$  can be obtained by solving Schrödinger equation, with charmonium potential to be its internal energy  $V=U$  [20]. The divergence of mean radius of

charmonium at  $T \rightarrow T_d$  indicates the melting of bound states. The value of  $T_d(J/\psi)$  is slightly above the region where photo-dissociation of  $J/\psi$  can be employed. At  $T > T_d$ , All charmonium is melt in this approach. Elastic collisions between charmonium and the hot medium have been checked [21] and found to be negligible for  $J/\psi$   $p_T$ -integrated observables.

During the evolution of QGP, uncorrelated  $c$  and  $\bar{c}$  from different  $c\bar{c}$  pairs may combine to form a new charmonium, which is called ‘‘regeneration’’ [15, 22]. The regeneration rate is represented by the term  $\beta_\Psi$  in Eq.(1), and it can be obtained from  $\alpha_\Psi$  by detailed balance [23]. The yield of regenerated charmonium is roughly proportional to  $N_{c\bar{c}}^2$ . Therefore at high colliding energies as LHC where  $N_{c\bar{c}}$  is large, the yield of regenerated charmonium becomes important (even dominates) in the final yields of charmonium [24–26]. Both initially produced charmonium and regenerated charmonium suffer suppression in QGP. At LHC colliding energies, QGP dominates the charmonium evolution and hadron phase contribution can be neglected.

Charm quark takes some time to reach thermal momentum distribution, due to its large mass [27]. In the beginning of QGP evolution, charm quark momentum distribution should be non-equilibrium. At this time, the initial temperature of QGP is much higher ( $T_{\text{QGP}} > T_d(J/\psi)$ ), where charmonium regeneration can not happens (all the charmonium is melt at  $T > T_d$ ). Only when the temperature of QGP drops below  $T_d(J/\psi)$ , the regenerated charmonium can survive. At the time where charmonium regeneration happens, charm quark should be closer to the thermal momentum distribution, compared with their initial distribution. Also, D meson elliptic flow is comparable with that of light hadrons [28, 29], one can take the thermal momentum distribution of charm quarks in QGP. The non-equilibrium of charm momentum distribution will suppress the yields of regenerated charmonium [17]. At forward rapidity bin, the regeneration will be more suppressed by this non-equilibrium effect. And the decreasing tendency of solid line in Fig.3 will be slightly enhanced.

With the conservation of total number of charm pairs during the evolution of QGP, its spatial density evolution satisfies the conservation law,  $\partial_\mu(\rho_c u^\mu) = 0$ . Charm quark initial spatial distribution is obtained by nuclear geometry,

$$\rho_c(\mathbf{x}_T, \eta, \tau_0) = \frac{d\sigma_{c\bar{c}}^{pp}}{d\eta} \frac{T_A(\mathbf{x}_T)T_B(\mathbf{x}_T - \mathbf{b}) \cosh(\eta)}{\tau_0} \quad (3)$$

where  $d\sigma_{c\bar{c}}^{pp}/d\eta$  is rapidity distribution of charm pairs produced in pp collisions,  $T_A$  and  $T_B$  are thickness functions of two colliding nuclei. It is defined as  $T_{A(B)}(\mathbf{x}_T) = \int_{-\infty}^{\infty} dz \rho_{A(B)}(\mathbf{x}_T, z)$ , and  $\rho_{A(B)}(\mathbf{x}_T, z)$  is Woods-Saxon nuclear density.

### III. COLD NUCLEAR MATTER EFFECTS

Initially produced charmonium is included as an input of Eq.(1). With cold nuclear matter effects, charmonium initial distribution at  $\tau = \tau_0$  in Pb+Pb collisions is,

sions is,

$$f_\Psi^{\text{init}}(\mathbf{x}, \mathbf{p}|\mathbf{b}) = \frac{(2\pi)^3}{E_T \tau_0} \int dz_A dz_B \rho_A(\mathbf{x}_T, z_A) \rho_B(\mathbf{x}_T - \mathbf{b}, z_B) \\ \times R_g^{Pb}(x_1, Q^2, \mathbf{x}_T) R_g^{Pb}(x_2, Q^2, \mathbf{x}_T - \mathbf{b}) \\ \times f_\Psi^{pp+\text{cronin}}(\mathbf{x}_T, \mathbf{p}, z_A, z_B|\mathbf{b}) \quad (4)$$

$R_g^{Pb}(x_{1,2}, Q^2, \mathbf{x}_T)$  is the gluon shadowing function from EKS98 package with transverse coordinate dependence [30, 31]. The relations between charmonium momentum and  $(x_{1,2}, Q^2)$  are  $x_{1,2} = (m_T/\sqrt{s_{NN}}) \exp(\pm y)$ , and  $Q^2 = m_T^2$  [32]. When two nuclei collide with each other, gluons may obtain extra energy by multi-scatterings with nucleons before fusing into a charmonium. This effect (called Cronin effect) results in the  $p_T$ -broadening of charmonium  $\Delta\langle p_T^2 \rangle = \langle p_T^2 \rangle_{pA} - \langle p_T^2 \rangle_{pp}$  [33]. It can be implemented by Gaussian smearing over the power-law  $p_T$ -spectra from pp collisions [8],

$$f_\Psi^{pp+\text{cronin}} = \frac{1}{\pi \Delta\langle p_T^2 \rangle} \int d\mathbf{p}_T'^2 \exp\left(-\frac{\mathbf{p}_T'^2}{\Delta\langle p_T^2 \rangle}\right) f_\Psi^{pp}(|\mathbf{p}_T - \mathbf{p}_T'|, p_z) \quad (5)$$

$f_\Psi^{pp}$  is the charmonium momentum distribution in free proton-proton collisions.  $\Delta\langle p_T^2 \rangle = a_{gN} \cdot \langle l \rangle$  where  $\langle l \rangle$  represents the mean nuclear path length before gluons fusing into  $\Psi$  [34], and the coefficient is extracted as  $a_{gN} = 0.15 \text{ GeV}^2/\text{fm}$  [26, 35]. For the charmonium momentum distribution in free pp collisions, it can be parametrized as

$$\frac{d^2\sigma_\Psi^{pp}}{dy p_T dp_T} = f_\Psi^{\text{Norm}}(p_T|y) \cdot \frac{d\sigma_\Psi^{pp}}{dy}(y) \quad (6)$$

$$f_\Psi^{\text{Norm}}(p_T|y) = \frac{(n-1)}{\pi(n-2)\langle p_T^2 \rangle_\Psi^{pp}(y)} \left(1 + \frac{p_T^2}{(n-2)\langle p_T^2 \rangle_\Psi^{pp}(y)}\right)^{-n} \quad (7)$$

with  $n = 4.0$ . In this work, I focus on the rapidity dependence of charmonium yield and momentum distribution. The rapidity dependence of charmonium yield is characterized by  $\frac{d\sigma_\Psi^{pp}}{dy}(y)$ .  $f_\Psi^{\text{Norm}}(p_T|y)$  is the charmonium transverse momentum distribution at different rapidity, normalized to unit. It depends on rapidity through the mean transverse momentum square  $\langle p_T^2 \rangle_\Psi^{pp}(y)$ . At PHENIX,  $\langle p_T^2 \rangle_\Psi^{pp}(y)$  is close to the form [36]

$$\langle p_T^2 \rangle_\Psi^{pp}(y) = \langle p_T^2 \rangle_\Psi^{pp}|_{y=0} \times \left[1 - \left(\frac{y}{y_{\text{max}}}\right)^2\right] \quad (8)$$

where  $y_{\text{max}} = \cosh^{-1}(\sqrt{s_{NN}}/(2m_T))$  is the maximum rapidity of charmonium in pp collisions. At the maximum rapidity, charmonium transverse momentum is small (close to zero) compared with  $m_\Psi$ , so one can take the approximation  $m_T \approx m_\Psi$  in the calculation of  $y_{\text{max}}$ . At LHC  $\sqrt{s_{NN}} = 2.76 \text{ TeV}$  pp collisions, I also take this parametrization and  $\langle p_T^2 \rangle_\Psi^{pp}|_{y=0} = 10 \text{ (GeV/c)}^2$  for  $J/\psi$  [37]. Initial distributions of excited states ( $\chi_c, \psi'$ ) are taken the same as  $J/\psi$ 's for simplicity. As charm quarks tend to be thermalized in QGP, final charmonium observables are almost not affected by charm quark initial momentum distribution. From EKS98 package, shadowing effect roughly reduces the total yield of charm pairs by around 20%, and this effect also shows weak rapidity dependence in Pb+Pb collisions [31].

The initial inclusive  $J/\psi$  production cross section with rapidity in  $\sqrt{s_{NN}} = 2.76 \text{ TeV}$  pp collision is measured by ALICE Collaboration at central and forward

rapidity regions [37], it is parameterized in Fig.1. Considering total prompt charmonium yield is about 90% of the inclusive yield in pp collisions, the cross section of prompt charmonium can be taken as  $0.9 \times \frac{d\sigma_{J/\psi}^{pp}}{dy}$ . In each  $p_T$  bin, the fractions of non-prompt  $J/\psi$  from B decay contribution can be extracted from [38].

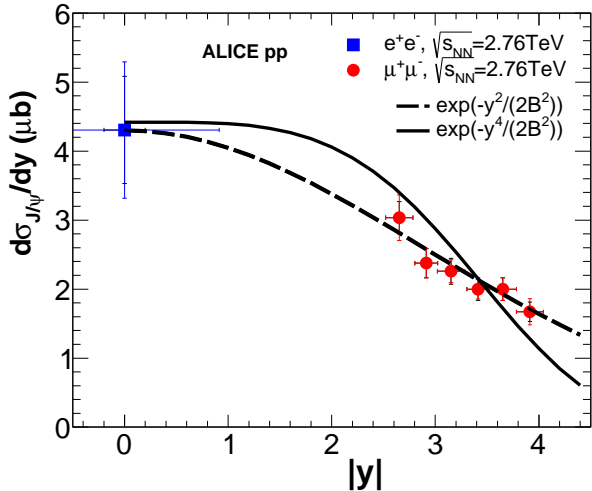


FIG. 1: (Color online) Differential inclusive  $J/\psi$  production cross section at  $\sqrt{s_{NN}} = 2.76$  TeV pp collisions, fitted by exponential functions  $\frac{d\sigma_{J/\psi}^{pp}}{dy} = A \exp(-y^n/(2B^2))$ . Solid and dashed lines correspond to  $n = 4$  and  $n = 2$  respectively. The parameters  $A$  and  $B$  are listed in table I. Data is from ALICE Collaboration [37].

TABLE I: parameters of  $\frac{d\sigma_{J/\psi}^{pp}}{dy}(y)$  in Fig.1

	$A$ ( $\mu b$ )	$B$
solid line	4.42	9.71
dashed line	4.30	2.88

At LHC colliding energies, the yield of initially produced charmonium are strongly suppressed by QGP due to color screening and gluon dissociation. The regenerated charmonium from charm and anti-charm quark recombination dominates the final yield of  $J/\psi$  in the low  $p_T$  bins. The yield of regenerated charmonium is roughly proportional to the square of charm quark density. Therefore different parameterization of  $\frac{d\sigma_{J/\psi}^{pp}}{dy}(y)$  and  $\frac{d\sigma_{c\bar{c}}^{pp}}{dy}(y)$  will result in different shape of  $R_{AA}^{J/\psi}(y)$ . In order to consider the uncertainties in Fig.1, I give two scenarios of  $\frac{d\sigma_{J/\psi}^{pp}}{dy}(y)$  with slowly decreasing (dashed line) and rapidly decreasing (solid line) tendencies in the region  $2 < |y| < 4$  (this is the region where  $R_{AA}^{J/\psi}(y)$  shows strong decreasing tendency in Fig.3). Even dashed line seems to fit data better in Fig.1, however, pQCD calculations indicate that at LHC colliding energies, the flat region of  $\frac{d\sigma_{c\bar{c}}^{pp}}{dy}$  can be as large as  $|y| < 3$  at  $\sqrt{s_{NN}} = 5.5$  TeV pp collisions [39], which supports the solid line in Fig.1. Both situations will be considered below. I use the same parametrization for charm pair production cross section,  $\frac{d\sigma_{c\bar{c}}^{pp}}{dy}(y) = S \times \frac{d\sigma_{J/\psi}^{pp}}{dy}(y)$ ,

and  $S$  is a constant. Only the data of total charm pair cross section  $\sigma_{c\bar{c}}^{\text{total}} = 4.8_{-2.76}^{+4.66}$  mb and  $\frac{d\sigma_{c\bar{c}}^{pp}}{dy}(|y| < 0.5)$  (with large error-bar) are available from ALICE Collaboration [40]. Lack of more constraint, I fit the  $J/\psi$  nuclear modification factor  $R_{AA}^{J/\psi}(N_p)$  in central rapidity region [26] by setting  $\frac{d\sigma_{c\bar{c}}^{pp}}{dy}(y = 0) = 0.85$  mb, which is also close to the cross section from FONLL model [26, 41]. It results in  $S = 0.85\text{mb}/A$  ( $A$  given in table I).

The inclusive nuclear modification factor of charmonium is defined as

$$R_{AA}^{\Psi}(\text{inclusive}) = \frac{N_{AA}^{\Psi}(\text{init}) + N_{AA}^{\Psi}(\text{rege}) + N_{AA}^{\text{B} \rightarrow \Psi}}{(N_{pp}^{\Psi} + N_{pp}^{\text{B} \rightarrow \Psi}) \cdot N_{\text{coll}}} = R_{AA}^{\text{init}} + R_{AA}^{\text{rege}} + R_{AA}^{\text{B} \rightarrow \Psi} \quad (9)$$

$N_{AA}^{\Psi}(\text{init, rege, B} \rightarrow \Psi)$  is the yield of  $\Psi$  from (initial production, regeneration, B hadron decay) respectively in nucleus-nucleus collisions.  $N_{pp}^{\Psi}$  is the yield of  $\Psi$  in pp collisions.  $N_{\text{coll}}$  is the number of binary collisions at fixed impact parameter  $\mathbf{b}$ . In the Eq.(9), all the denominators of three terms ( $R_{AA}^{\text{init}}$ ,  $R_{AA}^{\text{rege}}$ ,  $R_{AA}^{\text{B} \rightarrow \Psi}$ ) are  $(N_{pp}^{\Psi} + N_{pp}^{\text{B} \rightarrow \Psi}) \cdot N_{\text{coll}}$ .

In calculations before, transport model successfully explains the nuclear modification factor  $R_{AA}$  for charmonium [13, 26] and bottomonium [42], and also the excited state double ratio  $R_{AA}^{\psi'}/R_{AA}^{J/\psi}$  [43] with centrality, with (2+1)D ideal hydrodynamics and boost-invariant approximation in longitudinal direction. In this work, I employ the (3+1)D ideal hydrodynamics [44] and show the different mechanisms of  $J/\psi$  production at different rapidity regions.

#### IV. RAPIDITY DEPENDENCE

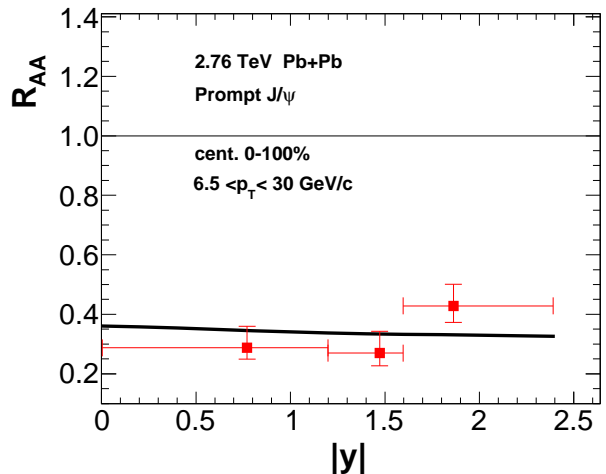


FIG. 2: (Color online) The prompt  $J/\psi$  nuclear modification factor as a function of rapidity for  $\sqrt{s_{NN}} = 2.76$  TeV Pb+Pb collisions. The data is from the CMS Collaboration [38].

In large transverse momentum bin  $6.5 < p_T < 30$  GeV/c, charmonium produced from parton hard scatterings at the nucleus colliding time ( $\tau = 0$ ) dominates

the final total yields of  $J/\psi$ . The regenerated charmonium are produced from the recombination of thermalized charm quarks and their transverse momentum is much smaller ( $\langle p_T^{\text{regeneration}}(J/\psi) \rangle \sim 2 \text{ GeV}/c$ ). Therefore the contribution of charmonium regeneration is almost zero in Fig.2 [45]. The line includes both cold and hot nuclear matter effects. Cold nuclear matter effects show weak rapidity dependence. For hot nuclear matter effects, the evolutions of the medium are similar at different rapidity, due to the boost invariance of the hot medium in central rapidity region. This results in a similar charmonium suppression at different rapidity and so the flat feature of  $R_{AA}^{J/\psi}(y)$ .

The situation is so different when coming to the entire  $p_T$  bin in Fig.3. Cold nuclear matter effects can not explain the decreasing tendency of  $R_{AA}$  in forward rapidity region  $2.5 < |y| < 4$ . Even shadowing effect shows strong rapidity dependence in p+Pb collisions, it shows very weak rapidity dependence in Pb+Pb collisions, see the results of EPS09 and nDSg models in Fig.3. The rapidity dependence of  $J/\psi$  observables in Pb+Pb collisions at LHC energies are mainly caused by hot medium effects. In  $p_T > 0$  bin in Fig.3, charmonium regeneration contributes more than half of the final total yields, and the decrease of regenerated charmonium yields results in the decreasing tendency of  $R_{AA}(y)$ .

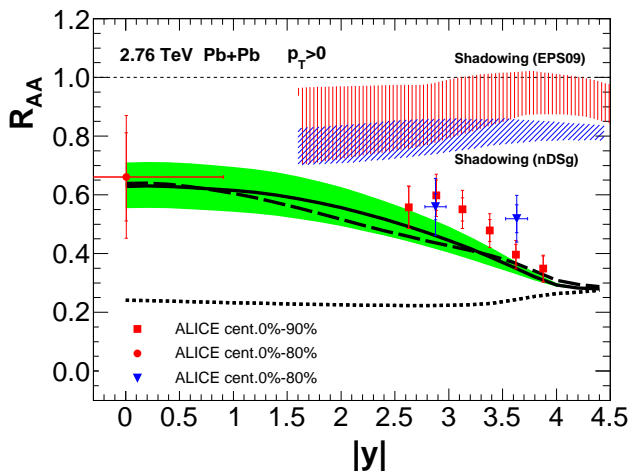


FIG. 3: (Color online) The inclusive  $J/\psi$  nuclear modification factor as a function of rapidity for  $\sqrt{s_{NN}} = 2.76 \text{ TeV}$  Pb+Pb collisions. Theoretical calculations are in centrality 0-90%. Dotted line includes initially produced charmonium and non-prompt charmonium (B decay), with both cold and hot nuclear matter effects. Black solid line and black dashed line are the total yields of charmonium with both cold and hot nuclear matter effects. They correspond to the cross sections of solid line and dashed line respectively in Fig.1. For the black solid line, I also shift  $\frac{d\sigma_{cc}^{pp}}{dy}(y)$  with 10% to consider the uncertainty of charm pair cross section, which results in the green color region of  $R_{AA}$ . Results of EPS09 and nDSg models are cited from [11]. The experimental data are from the ALICE Collaboration [11, 46].

Experimental data gives the inclusive  $J/\psi$  yield which includes non-prompt  $J/\psi$  from B hadron decay, and it contributes about 10% to the final inclusive yield

of  $J/\psi$ . Instead of calculating each centralities of the experimental data in Fig.3, I do the theoretical calculations in centrality 0-90%. The total nuclear modification factor is  $R_{AA}(y) = R_{AA}^{\text{init}}(y) + R_{AA}^{\text{rege}}(y) + R_{AA}^{B \rightarrow \Psi}(y)$ , see Eq.(9). In central rapidity region, the produced hot medium is boost invariant. This results in a flat tendency of  $R_{AA}^{\text{init}}(y)$  in Fig.3, similar with the line in Fig.2. In forward rapidity region, with rapidity increasing, the temperature of the medium decreases, and so  $R_{AA}^{\text{init}}(y)$  increases a little with rapidity (dotted line). The charm pair cross section decreases with rapidity (see Fig.1). It makes  $R_{AA}^{\text{rege}}(y)$  decreases with rapidity, and results in the decreasing tendency of  $R_{AA}(y)$  at forward rapidity region. Here, I give two results of  $R_{AA}(y)$  with different parametrization of  $\frac{d\sigma_{cc}^{pp}}{dy}(y)$  and  $\frac{d\sigma_{J/\psi}^{pp}}{dy}(y)$ . The form of  $\frac{d\sigma_{cc}^{pp}}{dy}(y) = A \exp(-y^4/(2B^2))$  decrease slowly with rapidity in central rapidity region  $|y| < 2$ , and decrease rapidly in forward rapidity region  $2.5 < |y| < 4$ . It results in the flat tendency of total nuclear modification factor  $R_{AA}$  in central rapidity region, and the strong decreasing tendency in forward rapidity region. Black dashed line is for  $R_{AA}$  with the charm pair cross section  $\frac{d\sigma_{cc}^{pp}}{dy}(y) = A \exp(-y^2/(2B^2))$ .

Considering the large error-bar of total charm pair cross section  $\sigma_{cc}^{pp}(\text{total})$ , I shift  $\frac{d\sigma_{cc}^{pp}}{dy}(y)$  up and down with 10% to consider the uncertainty, It results in the uncertainty of  $R_{AA}(y)$  shown as green color region in Fig.3.

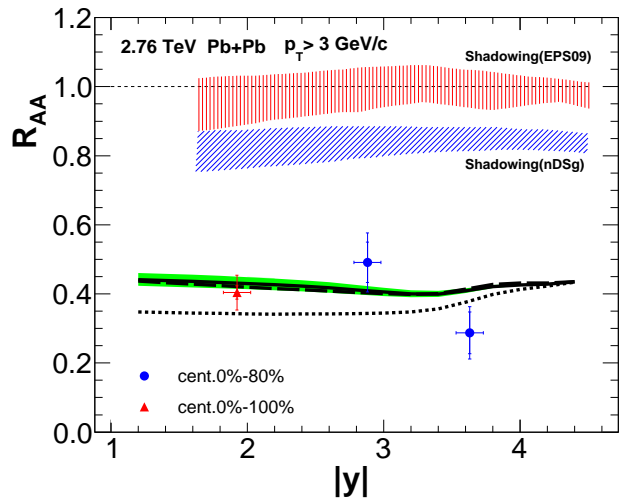


FIG. 4: (Color online) The inclusive  $J/\psi$  nuclear modification factor in  $p_T > 3 \text{ GeV}/c$  region as a function of rapidity for  $\sqrt{s_{NN}} = 2.76 \text{ TeV}$  Pb+Pb collisions. Theoretical calculations are in centrality 0-90%. Black dotted line, dashed line, solid line and green color region are the same with those in Fig.3, but in  $p_T > 3 \text{ GeV}/c$ . Results of EPS09 and nDSg models are cited from [11]. The experimental data are from the ALICE Collaboration [11].

This decreasing tendency of  $R_{AA}(y)$  is not so obvious in the data of the middle  $p_T$  bin of  $J/\psi$  in Fig.4, with only three data points and relatively large error bar. In this  $p_T$  bin, the fraction of B decay contribution in the final inclusive  $J/\psi$  yield is about 15% [38]. In Fig.4, there is also a flat region of  $R_{AA}$  in middle rapidity.

A small decreasing tendency of  $R_{AA}$  in  $2 < |y| < 3.5$  is caused by the decrease of charmonium regeneration. As regenerated charmonium is from the recombination of thermalized charm and anti-charm quarks, they are mainly distributed in low  $p_T$  bin. Therefore in middle  $p_T$  bin in Fig.4, the decrease of regenerated charmonium yield only results in a weak decreasing tendency of total nuclear modification factor  $R_{AA}$ . In  $y \geq 3.5$ , temperature of the medium decreases faster with rapidity, due to the end of boost invariance of hot medium. This gives less suppression of initially produced charmonium, and increase the  $R_{AA}^{\text{init}}(y)$  a little, see the dotted line. The competition between the increase of  $R_{AA}^{\text{init}}(y)$  and the decrease of  $R_{AA}^{\text{regc}}(y)$  results in the behavior of  $R_{AA}(y)$  in  $3 < |y| < 4$  region. Green color region is caused by the uncertainty of  $\frac{d\sigma_{c\bar{c}}^{pp}}{dy}(y)$ . With only shadowing effects,  $R_{AA}$  are far above the experimental data, please see Fig.4.

Even the rapidity dependence of prompt and inclusive  $J/\psi$  nuclear modification factor  $R_{AA}$  are well described at different transverse momentum bins, the theoretical calculations underestimate the elliptic flow of  $J/\psi$  in Fig.5. In  $p_T > 6.5$  GeV/c bin, initially produced  $J/\psi$  dominates the final yield. They are produced isotropically. However, the hot medium is anisotropic in centrality 0-60%, and so the suppression of charmonium is different when they move in different directions in the hot medium. This results in small elliptic flow of  $J/\psi$ . In Fig.5, I employ both smooth (3+1)D ideal hydro (black solid line) and smooth (2+1)D viscous hydro (red dashed line) for the theoretical calculations. Both of them underestimate the experimental data. In the transport model,  $J/\psi$  is assumed to move with constant velocity in QGP due to its large mass, this may underestimate its collective flows in high  $p_T$  bin. New mechanism of interactions between  $J/\psi$  and QGP may give additional enhancement of  $v_2$  in Fig.5 [47].

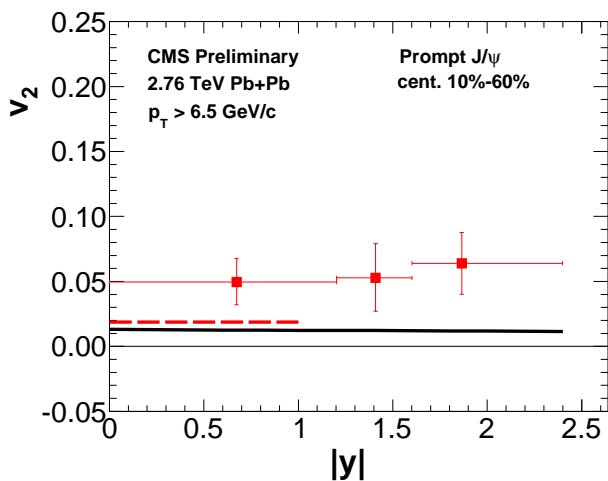


FIG. 5: (Color online) The elliptic flow of prompt  $J/\psi$  as a function of rapidity for  $\sqrt{s_{NN}} = 2.76$  TeV Pb+Pb collisions. The black line is for smooth (3+1)D ideal hydro, and red dashed line is for smooth (2+1)D viscous hydro. The data is from the CMS Collaboration [48].

In order to distinguish the  $J/\psi$  production mechanisms at different rapidity, I also calculate the ratio of  $J/\psi$  mean transverse momentum square in nucleus-nucleus collisions to that in proton-proton collisions  $r_{AA} = \langle p_T^2 \rangle_{PbPb} / \langle p_T^2 \rangle_{pp}$ . The mean transverse momentum of charmonium from parton hard scatterings (charmonium initial production) is much larger. The regenerated charmonium is from the recombination of thermalized charm and anti-charm quarks, and so the mean transverse momentum of charmonium is much smaller. In central rapidity region of Fig.6, The yield of regenerated charmonium dominates the final total yields of charmonium, due to the large charm pair cross section  $\frac{d\sigma_{c\bar{c}}^{pp}}{dy}(y)$ . It pulls down the mean transverse momentum square of final total  $J/\psi$ , and makes  $r_{AA} < 1$ . With rapidity increasing, the fractions of charmonium yields from regeneration decrease. This increases the  $\langle p_T^2 \rangle_{PbPb}$ . Also, the temperature of hot medium is smaller in forward rapidity region, which gives less suppression of charmonium. The fractions of charmonium initial production increases in final total yields. Unlike  $R_{AA}$ , both of above effects increase the  $r_{AA}$ , which makes  $r_{AA}$  more sensitive to the mechanisms of charmonium production in hot medium. In  $|y| > 3.8$ ,  $\langle p_T^2 \rangle_{AA}$  is larger than  $\langle p_T^2 \rangle_{pp}$ . This is caused by the leakage effect: charmonium with larger momentum suffer less suppression in hot medium, which increases the mean transverse momentum square of final total  $J/\psi$  in Pb+Pb collisions and makes  $r_{AA} > 1$ .

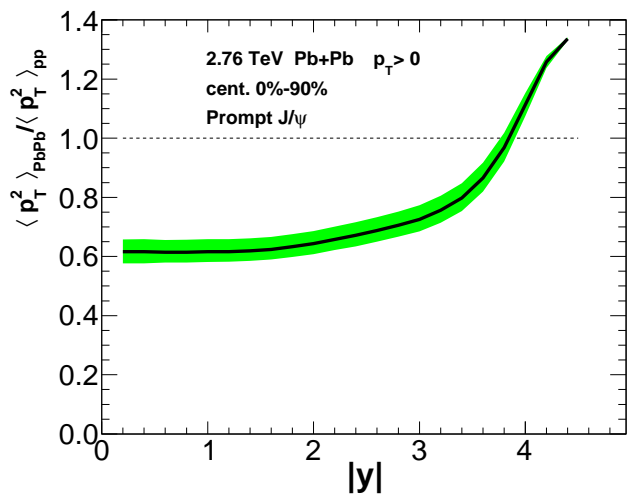


FIG. 6: (Color online) The mean transverse momentum square ratio  $r_{AA}$  of prompt  $J/\psi$  as a function of rapidity for  $\sqrt{s_{NN}} = 2.76$  TeV Pb+Pb collisions. Theoretical calculations are in the centrality 0-90%. Black solid line and green color region are the same with those in Fig.3.

## V. CONCLUSION

In summary, I employ both (3+1) dimensional Boltzmann-type transport equation and hydrodynamics to calculate the detailed rapidity dependence of  $J/\psi$  nuclear modification factor  $R_{AA}(y)$  and the ratio of mean transverse momentum square  $r_{AA}(y)$  at

LHC  $\sqrt{s_{NN}} = 2.76$  TeV Pb+Pb collisions. Different from p+Pb collisions, in Pb+Pb collisions cold nuclear matter effects are almost independent of rapidity. Hot medium suppression from gluon dissociation shows weak rapidity dependence, due to boost invariance of the medium in central rapidity region. Both the strong decreasing tendency of  $R_{AA}$  and increasing tendency of  $r_{AA}$  in forward rapidity region are caused by the rapid decrease of regeneration contribution. The ratio of mean transverse momentum square  $r_{AA}$  seems more sensitive to the mechanisms of  $J/\psi$  production. Theoretical calculations explain the experimental data at high and middle  $p_T$  bin and also the strong decreasing tendency of  $R_{AA}(y)$  in entire  $p_T$  bin, but have some discrepancy with the data of  $J/\psi$  elliptic flow in Fig.5. More precise data and theoretical study are needed to understand the behavior of heavy flavor in the deconfined matter.

**Acknowledgement:** Author thanks Dr.Fuming Liu in CCNU for helpful discussions in the beginning of this work, and Dr.Pengfei Zhuang and Dr.Kai Zhou for the good suggestions in this work.

- 
- [1] T.Matsui and H.Satz, Phys. Lett. **B178**, 416(1986).  
[2] R. L. Thews, M. Schroedter and J. Rafelski, Phys. Rev. C **63**, 054905 (2001).  
[3] L. Grandchamp and R. Rapp, Nucl. Phys. A **709**, 415 (2002).  
[4] A. Andronic, P. Braun-Munzinger, K. Redlich and J. Stachel, Phys. Lett. B **571**, 36 (2003).  
[5] A. Andronic, P. Braun-Munzinger, K. Redlich and J. Stachel, J. Phys. G **38**, 124081 (2011).  
[6] A.Adare *et al.*, [PHENIX Collaboration], Phys. Rev. Lett. **98**, 232301(2007).  
[7] Y. Liu, Z. Qu, N. Xu and P. Zhuang, J. Phys. G **37**, 075110 (2010).  
[8] X. Zhao and R. Rapp, Eur. Phys. J. C **62**, 109 (2009).  
[9] B. Krouppa, R. Ryblewski and M. Strickland, Phys. Rev. C **92**, no. 6, 061901 (2015).  
[10] L.Manceau, [ALICE Collaboration], EPJ Web Conf. **60**, 13002 (2013).  
[11] B.Abelev *et al.*, [ALICE Collaboration], Phys. Rev. Lett. , **109**, 072301(2012).  
[12] A. Andronic, P. Braun-Munzinger, K. Redlich and J. Stachel, Phys. Lett. B **652**, 259 (2007).  
[13] X. l. Zhu, P. f. Zhuang and N. Xu, Phys. Lett. B **607**, 107 (2005).  
[14] Y. Liu, N. Xu and P. Zhuang, Nucl. Phys. A **834**, 317C (2010).  
[15] L. Grandchamp and R. Rapp, Phys. Lett. B **523**, 60 (2001).  
[16] L. Grandchamp, R. Rapp and G. E. Brown, Phys. Rev. Lett. **92**, 212301 (2004).  
[17] X. Zhao and R. Rapp, Phys. Rev. C **82**, 064905 (2010).  
[18] M.E.Peskin, Nucl. Phys. **B156**, 365(1979).  
[19] G.Bhanot, M.E.Peskin, Nucl. Phys. **B156**, 391(1979).  
[20] H.Satz, J. Phys. **G32**, R25(2006).  
[21] B. Chen, K. Zhou and P. Zhuang, Phys. Rev. C **86**, 034906 (2012).  
[22] R. L. Thews, M. Schroedter and J. Rafelski, J. Phys. G **27**, 715 (2001).  
[23] L.Yan, P.Zhuang, N.Xu, Phys. Rev. Lett **97**, 232301(2006).  
[24] X. Zhao and R. Rapp, Nucl. Phys. A **859**, 114 (2011).  
[25] X. Du and R. Rapp, Nucl. Phys. A **943**, 147 (2015).  
[26] K. Zhou, N. Xu, Z. Xu and P. Zhuang, Phys. Rev. C **89**, no. 5, 054911 (2014).  
[27] J. Zhao, A. Emerick and R. Rapp, Nucl. Phys. A **904-905**, 611c (2013).  
[28] A.Adare *et al.*, [PHENIX Collaboration], Phys. Rev. Lett. **98**, 172301(2007).  
[29] V. Greco, C. M. Ko and R. Rapp, Phys. Lett. B **595**, 202 (2004).  
[30] K. J. Eskola, V. J. Kolhinen and C. A. Salgado, Eur. Phys. J. C **9**, 61 (1999).  
[31] R. Vogt, Phys. Rev. C **81**, 044903 (2010).  
[32] R. Vogt, Phys. Rev. C **71**, 054902 (2005).  
[33] S.Gavin, M.Gyulassy, Phys. Lett. **B214**, 241(1988).  
[34] J. Hufner and P. f. Zhuang, Phys. Lett. B **515** (2001) 115.  
[35] R. L. Thews and M. L. Mangano, Phys. Rev. C **73**, 014904 (2006).  
[36] A.Adare, *et al.*, [PHENIX Collaboration], Phys. Rev. Lett. **98**, 232002(2007).  
[37] B. Abelev *et al.* [ALICE Collaboration], Phys. Lett. B **718**, 295 (2013).  
[38] S. Chatrchyan *et al.* [CMS Collaboration], JHEP **1205**, 063 (2012).  
[39] A. Andronic, P. Braun-Munzinger, K. Redlich and J. Stachel, Nucl. Phys. A **789**, 334 (2007).  
[40] [ALICE Collaboration], JHEP **1207**, 191(2012).  
[41] M. Cacciari, M. Greco and P. Nason, JHEP **9805**, 007 (1998); M. Cacciari, S. Frixione and P. Nason, JHEP **0103**, 006 (2001).  
[42] Y. Liu, B. Chen, N. Xu and P. Zhuang, Phys. Lett. B **697**, 32 (2011).  
[43] B. Chen, Y. Liu, K. Zhou and P. Zhuang, Phys. Lett. B **726**, 725 (2013).  
[44] T.Hirano, Phys. Rev. **C65**, 011901(2001).  
[45] X. Zhao and R. Rapp, Phys. Lett. B **664**, 253 (2008).  
[46] [ALICE Collaboration], Nucl. Phys. **A904**, 202c(2013)  
[47] B. Z. Kopeliovich, I. K. Potashnikova, I. Schmidt and M. Siddikov, Phys. Rev. C **91**, no. 2, 024911 (2015).  
[48] [CMS Collaboration], CMS-PAS-HIN-12-001(2013).